THE AUTOMATED DETECTION OF MAGNETIC FIELD INVERSION AND ITS CORRELATION WITH FILAMENT ELONGATION IN SOLAR IMAGES

V.V.Zharkova[1], S.S. Ipson[1], R.S.Qahwaji[2] , A.K. Benkhalil[1] and S.I. Zharkov[1]
1-Cybernetics Department, Bradford University, Bradford, BD7 1DP, UK
2-EIMC Department, Bradford University, Bradford, BD7 1DP, UK
Tel:+44 1274 232323; Fax: +44 1274 236600
e-mail: v.v.zharkova@Bradford.ac.uk

ABSTRACT

Filaments are prominences seen projected as dark features against the solar disk. They are normally found near neutral lines in the solar magnetic fields and have been used to map neutral lines in studies of the evolution of the solar magnetic field. This paper describes a fast automatic system for the detection of filaments using a sequence of morphological operations. Tests on solar images obtained from the Meudon observatory over a one month period showed error rates of between 7% and 12% compared with manual results. The paper also presents a new approach to constructing magnetic neutral lines, based on the Euclidean distance transform. The results obtained are compared with those obtained by applying Gaussian smoothing to solar magnetograms. With both methods the detailed shape of the neutral lines depends on one parameter, either a threshold or a smoothing radius. Generally good agreement between the positions of the filaments and neutral lines is obtained.

1 INTRODACTION

Filaments are the projections on a solar disk of prominences seen as very bright and large-scale features on the solar limb (for some examples see reference [1]) Their locations and shapes do not change very much over long periods and, hence, their lifetime is likely to be much longer then one solar rotation. However, there are visible changes in filament elongation, position with respect to an active region and relative to magnetic field configuration. Normally, filaments are elongated along neutral magnetic lines of the active regions; however, its magnetic field slightly deviates from zero to either positive or negative polarity. For this reason the automated detection of solar filaments and their confinement near the position of a relevant neutral magnetic line is a very important task to tackle in the sense of understanding the physics of prominence formation, support and disruption.

The aim here is to design a robust and efficient detection system that can extract the positions of filaments regardless of their shapes, positions or sizes. The detection is carried out using a hybrid-based system that combines edge-based techniques with region-based techniques. The detection system accepts a raw unprocessed image and processes it in order to determine the regions containing the filaments. The process is divided to three major steps: 1) the detection of the central solar region; 2) the detection of filament regions; 3) the detection of a magnetic field inversion; 4) the synchronisation of the two images.

2 THE FILAMENT DETECTION ALGORITHM

The automatic detection of filaments is carried out using three major stages. The central solar region is detected in the first stage. The morphological hit-miss transform, watershed transform and the Filling algorithm are implemented in this stage. Intensity filters and image enhancement techniques are implemented in the second stage to enhance the quality of detection in the central region. A Combination of mosaic technique and detection windows is implemented in the third stage to detect the positions of filaments and to define rectangular windows just containing them. The detected regions can be input later to a neural network for verification purposes. The major detection stages are shown in Figure 1.

The Filling algorithm, introduced in [2,3] is the corner stone for the detection of the central solar region. Originally, the Filling algorithm was designed to distinguish between a region that lies outside an object and a region that lies within an object [2, 3]. The algorithm depends on understanding the behaviour of a

morphological Hit-Miss transform and the Watershed algorithm (WST) inside the closed and open shape objects. The Filling algorithm detects the longest Watershed transform line that corresponds to a closed-shape region and reconstructs its object in order to obtain the solar disk. A detection threshold is added to reconstruct the central solar region only in order to avoid the handling regions that are located on the limb. In addition, the modified hexagonal Hit-Miss transform is implemented because it provides efficient and robust edge detection performance [4]. The practical implementation of the first stage is shown in Figure 2.

Figure 1. The major stages in the detection process

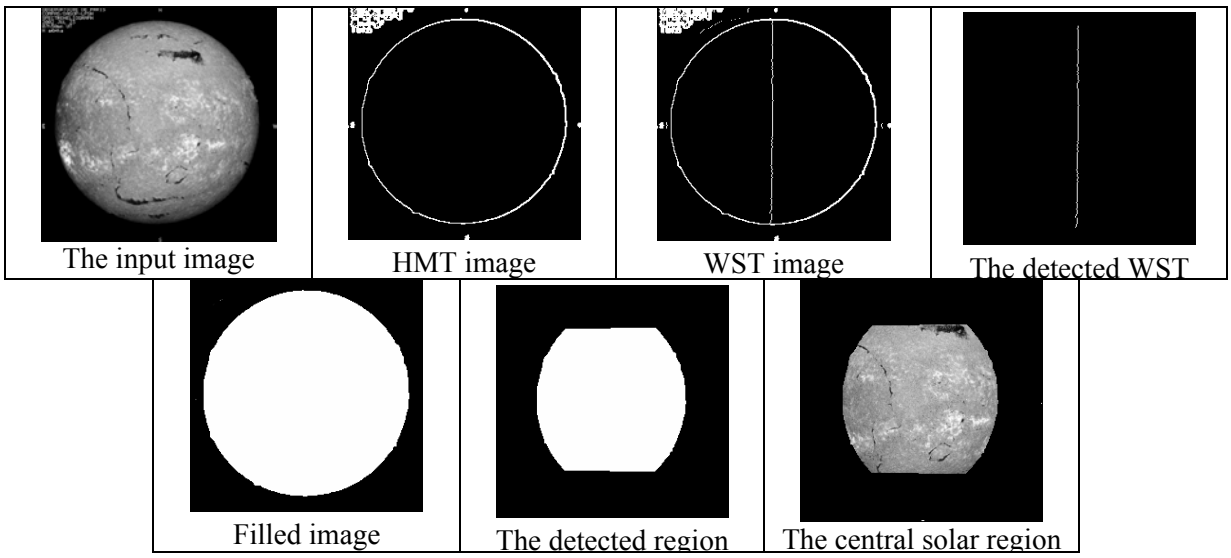

Figure 2. The intermediate images resulting from the implementation of the detection algorithm to the Halpha input image taken on 23rd July, 2002

After the central region is detected, image enhancement is applied followed by low intensity thresholding. Solar image enhancement aims to increase the grey-scale differences between the active regions and filaments, in order to facilitate the detection of filaments. This is implemented by finding the mean of the central region and finding the maximum and minimum grey scale values. The values of the pixels are re-calculated in order to maximise the differences with the mean without changing the mean's value. A new grey-level value that replaces the old value is computed. Intensity filtering using low thresholds is applied afterwards. The filaments and filaments-like regions are darker in colour which enables an intensity filter with a low threshold to indicate their positions and to eliminate background and active regions. The enhancement and filtering stage provides an image which contains the candidates of filaments as shown in Figure 3.

The final detection stage starts by sliding a window over the mosaic image. Every time the window reaches the upper edge of a mosaic filament a search for the lower, left and right boundaries for the filament region is carried out. The left boundaries are determined by searching the neighbourhood of the upper edge, which is located to the left. The left boundary is located at the vertical line that passes through the filament mosaic pixel, which has the maximum horizontal distance to the left. Similarly, the right boundary of the filament is detected. The horizontal row that passes through the filament pixels with the maximum vertical distance from the upper edge is considered to be the lower boundary. Once the boundaries of the filament are

determined, the filament pixels are painted in a false colour to prevent them from being detected again by another moving window. At the end of this process, a number of variable size windows are defined and stored in the multiple size arrays. The generated arrays contain the detected filaments, which are located inside the central solar region. The detected rectangular regions are extracted from the image and represented in a data file that could be fed to a neural network classifier to be verified as a filament region. The practical implementation of this stage is shown in Figure 4.

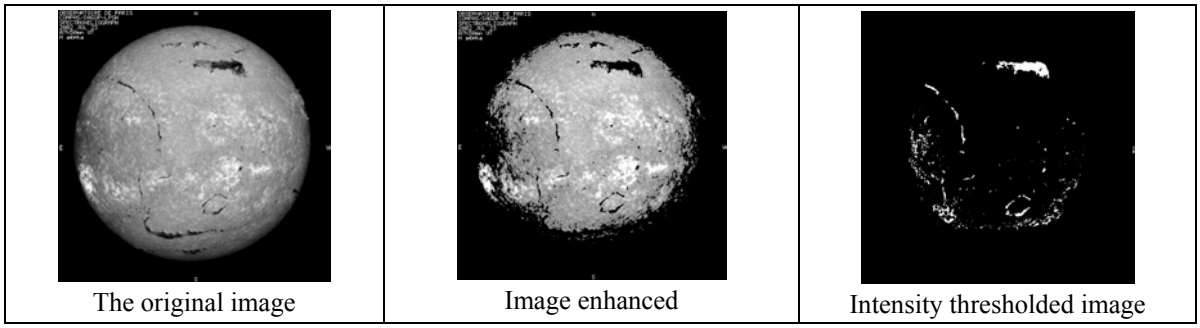

Figure 3. The practical implementation of the enhancement and filtering stages

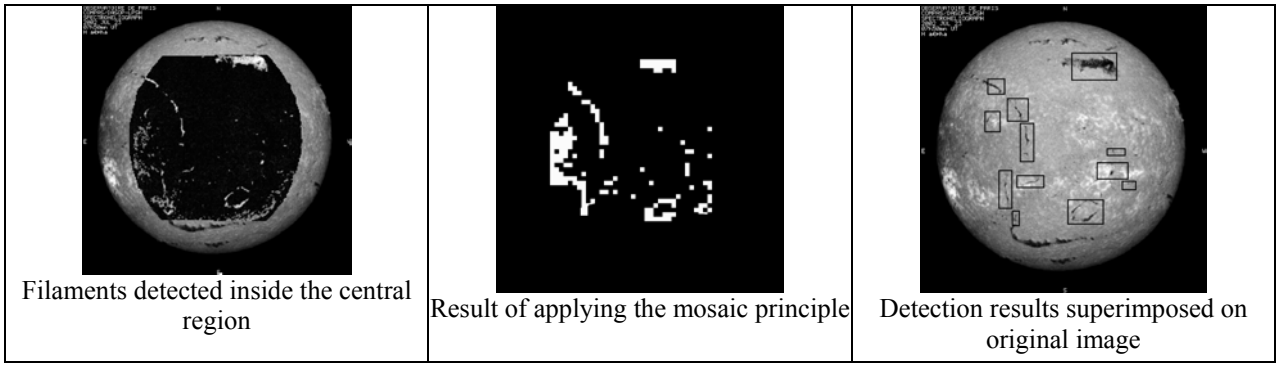

Figure 4. The practical implementation of the third detection stage

Practically, this algorithm was tested using H-alpha images from Meudon observatory. Two error rates were established, false acceptance rate (FAR) and false reject rate (FRR) [5]. FAR error rate relates to the detection of non-filaments regions that are considered to be filaments, while FRR error rate relates to the failure of the system to detect filaments. On the average, it is found that FAR error rate is 11.9% while the FRR error rate is 6.7%, when implemented on H-alpha images that are taken over one month. The detection algorithm is fast as it can handle more than one image per second and it provides robust performance under noise conditions because of the efficiency of the Filling algorithm and its morphological transforms.

3 Analysis of the magnetic inversion lines

It is well known that solar filaments are associated with magnetic inversion lines in the photosphere separating regions of positive and negative emerging magnetic field. There is considerable interest in automatically mapping inversion (sometimes called neutral) magnetic lines and investigating their evolution and relationships to other solar phenomena. Solar magnetograms are produced by a number of the ground and space based observatories. However, this paper is concerned with the comparison of filament images observed in H-alpha radiation with magnetograms produced by the Michelson Doppler Instrument (MDI) installed on the SOHO spacecraft. The magnetograms produced by this instrument provide an array of 1024 by 1024 pixel measurements of the line of sight component (the dominant component of the magnetic vector field in the central portion of the disk) of the solar magnetic field in the photosphere. The radius of the solar disc in these magnetograms is about 489 pixel (corresponding to a pixel resolution of about 2 arc sec) and the magnetograms are produced at a rate of one per minute

except during periods of occasional down-time. The magnetogram pixel values are stored using16 bits, with a signal range from about -1500 G to +1500 G and a noise level of about ±20 G.

Several studies [6, 7, 8] have shown that the general magnetic field of the sun consists of small (1-2 arc sec) but intense (~ 1200 G) flux knots of mixed polarity. In some regions the flux knots are fairly evenly distributed while in others one polarity dominates and at low resolution observation masks those of the other polarity to give what is often described as a unipolar region. In a typical example of an MDI magnetogram from SOHO the boundary between adjacent positive and negative magnetic regions is well defined only at comparatively few locations between local concentrations of opposite field associated with sun spots. Elsewhere, positive (and negative) regions are indicated by the presence of mainly positive (or negative) fluctuations from the ±20 G, near zero, range of magnetic field intensity defined by the noise level.

The boundaries between positive and negative regions of an MDI magnetogram generally have a great deal of fine structure, as is hinted at by the magnetograms shown at the top left corner in Figures 2 and 3 which have the minimum smoothing in the two sets of magnetograms. This fine detail can be reduced by local averaging of individual magnetograms (e.g. Durrant [9]) or by averaging, after differential rotation, all available magnetograms for a Carrington rotation (e.g. Ulrich et al. [10]). This paper examines another approach which is applied to a single magnetogram and is capable of retaining the structure of neutral line boundaries in high field regions, while reducing the fine detail elsewhere.

The principal idea for the automatic construction of boundary lines separating adjacent collections of small positive magnetic features from adjacent collections of small negative magnetic features is to grow the features isotropically (using a distance transform) and to mark the points where the positive and negative regions make contact. The resulting points are used as estimates of points along inversion lines. The initial seed regions are obtained by applying positive and negative thresholds of equal magnitude which defines the solar disk into three regions: positive regions, negative regions and neutral regions within which the neutral lines are found. The specific steps used to construct the inversions lines in this illustration are as follows.

The magnetogram data are first read from the fits file and stored in a floating point array. A 3 by 3 median filter is applied which reduces noise fluctuations without blurring the edges. The resulting floating point data is then segmented into the three types of magnetic regions by applying a two level magnetic field threshold ± T, where T could be set at the noise level 20 G say. A fast Euclidean distance transform [11] is applied to label the pixels in the neutral region with distance from the nearest segmented boundary pixel. On completion of the distance transform, each pixel in the neutral region is replaced by one of two labels to indicate whether the nearest boundary pixel is positive or negative. The boundaries between the positive and negative labelled regions (forming a Voronoi tessalation) indicate the estimated positions of the neutral lines. The neutral lines can be marked explicitly by applying an edge detector, to the image array containing the Voronoi tessalation.

The general affect that the value of threshold T has on the resulting neutral lines is illustrated by the sequence of images shown in Figure 5. From left to right along the top row and then from left to right along the bottom row, the threshold varies in steps of 5 G from 5 to 40 G. The result is a reduction in the number of regions and a simplification of the boundaries of the resulting regions except where the neutral line separates two strong regions of magnetic field. These latter sections of neutral lines can be identified in the images corresponding larger threshold values where the boundary retains fine structure. For comparison, a similar sequence of magnetograms, but with increasing amounts of Gaussian smoothing, is shown in Figure 6. No attempt has been made to make the smoothing applied to the individual magnetograms in Figure 6 correspond to the reduction in detail obtained by increasing the threshold value applied to the magnetograms in Figure 5. Nevertheless, over the central two thirds of the solar magnetograms, in the low field gradient regions, the reduction of detail as the smoothing or threshold value is increased produces similar results. Near the limb, the results are distorted by foreshortening of the spatial extent of the data and by boundary effects. Durrant [2002] is particularly concerned with mapping neutral lines in the Polar Regions which are near the limb and maps the observed magntograms to a latitude-longitude grid, applies smoothing on the grid and then maps the result back to the solar disk.

An example of the detected neutral lines, superimposed on the original magnetogram, is shown in Figure 7 (left). Figure 7 (right) shows an example of a set of inversion lines constructed in this way, superimposed on an H-alpha image which has been rescaled and registered to the size and position of the solar disc in the original magnetogram and enhanced to make the filaments more visible. It is evident from this figure that there is a strong correlation between the

locations of the filaments and the inversion lines. Close inspection of Figure 4 and either of Figure 5 or Figure 6 reveals a strong correlation positions of neutral lines and most of the filaments. This would be improved by taking the time difference of eight hours between the magnetogram and the H-alpha images into account. The biggest discrepancy is for the large and prominent filament near the top of the image. It lies in a region of positive magnetic polarity and only for lower smoothing/threshold values does its foot points appear close to neutral lines.

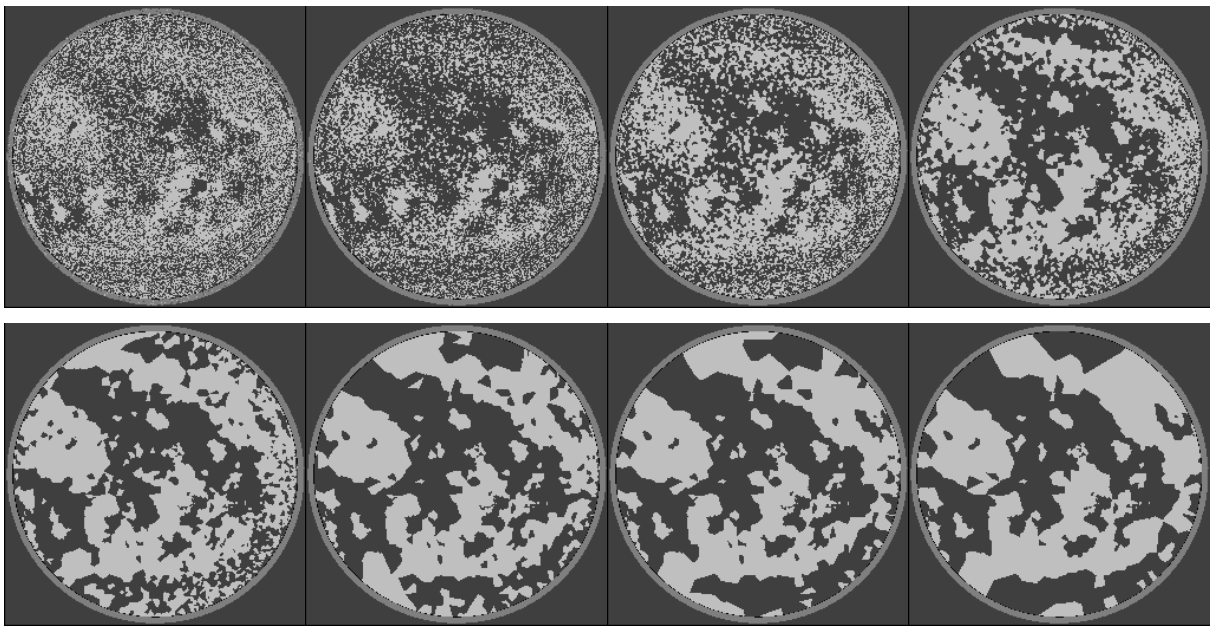

Figure 5 Neutral lines indicated by the boundary between dark (negative) and light (positive) regions for thresholds varying from 5 to 40 from top left bottom right. MDI July 23 2002

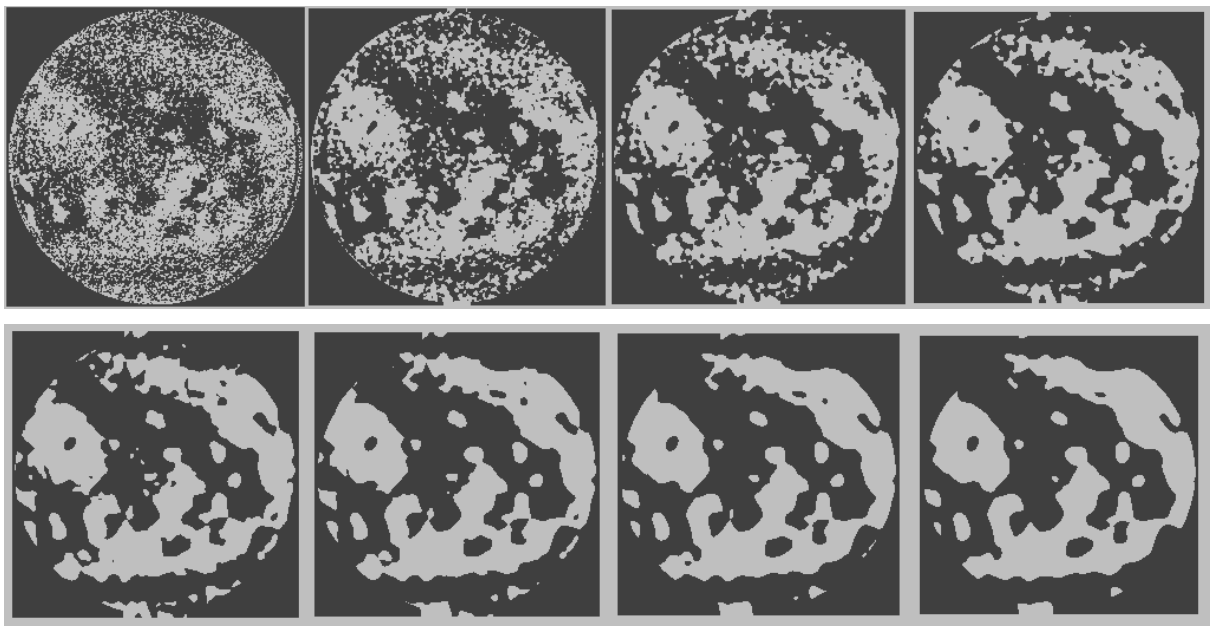

Figure 6 Neutral lines indicated by the boundary between dark (negative) and light (positive) regions for smoothing radii varying from 5 to 40 from top left bottom right. MDI July 23 2002

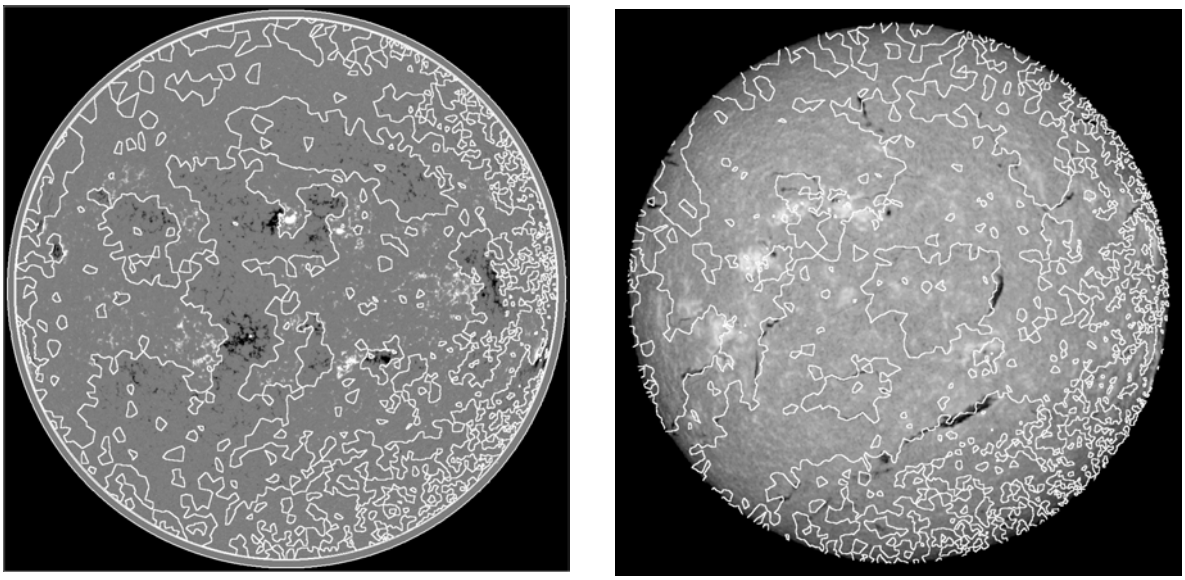

Figure 7 The composite image on the left (July 23 2002) shows magnetic neutral lines superimposed on the original magnetogram. The composite image on the right (April 21 2002) shows magnetic neutral lines superimposed on the corresponding H-alpha image within which filaments are visible as darker regions.

Conclusions

In this paper, a fast algorithm for the detection of filaments in solar images is described. The detection process consists of three major stages: the detection of a central solar region, initial detection using enhancement and intensity filtering and the final detection of filament regions. The algorithm is tested on solar images that are obtained from the Meudon observatory. These images cover the period from 1/ 7 / 2001 till 5/ 8/ 2001. The detection algorithm is fast and it provides an FAR error rate of 11.9% and FRR error rate of 6.7%, when compared against the detected filaments in the manually constructed synoptic maps. The detection algorithm is also tested against noise condition where robust performance is obtained. Two quite different methods of estimating the positions of magnetic neutral lines have been compared. The results found are similar although as the magnetograms are simplified, in one case by increasing smoothing and in the other by increasing threshold, one method retains fine structure in the regions of strong magnetic fields. In the cases examined most of the filaments are found to be close to neutral lines as suggested in previous literature. This research has been done for the European Grid of Solar Observations (EGSO) funded by the European Commission within the IST Fifth Framework, grant IST-2001-32409.

References

[1] Zharkova, V.V., Ipson, S. S., Zharkov, S.I., Benkhalil, A., Aboudarham, J., Bentley, R.D., "A full disk image standardisation of the synoptic solar observations at the Meudon Observatory", Solar Phys., vol. 214, No 1, pp.89-105, 2003.

[2] Qahwaji R. and Green R., "Detection of Closed Regions in Digital Images", International Journal of Computers and Their Applications, vol. 8, No. 4, pp. 202-207, 2001.

[3] Qahwaji R. and Green R., "Detection of Closed-Shape Objects", Journal of Information, vol.4, No. 4, pp. 429-434, 2001.

[4] Qahwaji R. , "Detecting Edges in Noisy Images", Accepted for Publications: International Journal of Computers and Their Applications, 2003.

[5] Hong L. and Jain A., "Integrating faces and fingerprints for personal identification", IEEE Transactions on Pattern Analysis and Machine Intelligence, vol. 20, No. 12, pp. 1295-1307, 1998.

[6] Severny, A., "The general magnetic field of the sun and its changes with time", Vistas Astron., vol. 13, pp. 135-148, 1972.

[7] Howard, R. F., “Large-scale solar magnetic fields “,Annual review of astronomy and astrophysics, vol. 15, pp. 153-173, 1977.

[8] Zwaan, C., “Elements and patterns in the solar magnetic field “, Annual review of astronomy and astrophysics, vol. 25, pp. 89-111, 1987.

[9] Durrant., C. J., “Polar magnetic fields – filaments and the zero-flux contour”, Solar Phys., vol. 211, pp. 83-102, 2002.

[10] Ulrich, R. K., Evens, S., Boyden. J. E., and Webster, L., “Mount Wilson synoptic magnetic fields: improved instrumentation, calibration and analysis applied to the 2000 July 14 flare and to the evolution of the dipole field”, Astrophysical Journal Supplement Series, vol. 139, No. 1, pp. 259-279, 2002.

[11] Cuisenaire, O. and Macq B., “Fast and exact signed Euclidean distance transformation with linear complexity”, In Proc. IEEE Int. Conference on Acoustics, Speech and Signal Processing (ICCASSP99), vol. 6, pp. 3293-3296, Phoenix (AZ), March 1999.